International Journal of Nanomedicine

Dovepress
open access to scientific and medical research

Open Access Full Text Article

ORIGINAL RESEARCH

Poly(ε-Caprolactone)-Methoxypolyethylene Glycol (PCL-MPEG)-Based Micelles for Drug-Delivery: The Effect of PCL Chain Length on Blood Components, Phagocytosis, and Biodistribution

Zemin Hou[1,2,*], Wencheng Zhou[1,2,*], Xi Guo[2], Rui Zhong[3], Ao Wang[4], Jiehua Li[4], Ying Cen[1], Chao You[2], Hong Tan[4], Meng Tian[2]

[1]Department of Burn and Plastic Surgery, National Clinical Research Center for Geriatrics, West China Hospital, Sichuan University, Chengdu, Sichuan, People's Republic of China; [2]Department of Neurosurgery and Neurosurgery Research Laboratory, West China Hospital, Sichuan University, Chengdu, Sichuan, People's Republic of China; [3]Institute of Blood Transfusion, Chinese Academy of Medical Science & Peking Union Medical College, Chengdu, Sichuan, People's Republic of China; [4]College of Polymer Science and Engineering, State Key Laboratory of Polymer Materials Engineering, Sichuan University, Chengdu, Sichuan, People's Republic of China

*These authors contributed equally to this work

Correspondence: Meng Tian, Department of Neurosurgery and Neurosurgery Research Laboratory, West China Hospital, Sichuan University, No. 37 Guoxue Alley, Wuhou District, Chengdu, Sichuan Province, 610041, People's Republic of China, Tel +86 28 85164168, Email tianmeng@scu.edu.cn

Background: The main challenge of polymeric micelles as drug delivery systems is that the actual delivery efficiency is not as high as expected, which is closely related with the interactions with the complex biological environments such as blood components, phagocytosis, and biodistribution. Herein, we expect to understand these concerns for the clinically relevant micelles that composed of methoxypolyethylene glycol (MPEG) with identical chain length And poly(ε-caprolactone) (PCL) with tunable chain length (PCL_n-MPEG) (n=20, 30, and 40) wherein doxorubicin was encapsulated as a model drug.

Methods: The doxorubicin-loaded PCL_n-MPEG micelles were prepared by a dialysis method and characterized by dynamic light scattering and transmission electron microscopy. The surface PEG density and chain conformation were investigated by dissipative particle dynamics simulation. The stability of the micelles was detected by nanoparticle tracking analysis. The effects of PCL chain length on the blood components, phagocytosis, and biodistribution were assayed in vitro and in vivo.

Results: The micelles exhibited spherical morphology with a diameter about 30nm. The PEG chain conformation from "mushroom-like" to "brush-like" was evident. The micelles have no remarkable effect on the red blood cells, blood coagulation, and platelet activation. Interestingly, the protein adsorption was affected and dependent on the chain conformation, with lowest adsorption for PCL_{30}-MPEG, which also has the loWest phagocytosis. The stability of the micelles was in the order of PCL_{40}-MPEG>PCL_{30}-MPEG>PCL_{20}-MPEG which was dependent on the PCL chain length. The micelles mainly accumulated in liver, with the order consistent with their stability, indicating that, besides the phagocytosis, the stability of the micelle plays an important role in biodistribution as well. The related mechanisms were proposed and discussed.

Conclusion: Manipulating the PEG/PCL ratio of the micelle is an effective approach to modulate the protein adsorption, phagocytosis, and biodistribution, which may be a prerequisite for clinical applications.

Keywords: micelles, blood components, phagocytosis, biodistribution

Introduction

One of the ideal goals when administering medication to patients is to enhance curative efficiency while limiting drug toxicity and side effects at non-diseased sites. Nanocarriers such as polymeric micelles continue to receive considerable attentions for drug delivery as they effectively prolong circulating half-life of drugs as well as allow for lower dosages and less frequency of administration so that relieve the adverse effects through their tunable physicochemical

Received: 26 November 2021
Accepted: 7 March 2022
Published: 5 April 2022

properties.[1–3] For example, in Gao's research, a newly developed docetaxel loaded poly(2-oxazoline) amphiphilic micelles showed high stability, high drug loading content up to 25% against the docetaxel and demonstrated better antitumor effect than docetaxel injection.[4] Similarly, Wu et al recently developed poly (salicylic acid) (PSA) nanoparticles (NPs) with prickly structures and demonstrated that drug-loaded PSA NPs effectively targeted at tumor sites and prolonged circulation time.[5]

However, up to now, the treatment efficacy in clinic is not as effective as expected, eg, the amount of drug accumulated in the lesion is less than 10% of the systemic administered dose, and in most cases there is no therapeutic advantages over free drugs such as paclitaxel loaded polyethylene glycol-poly (D,L-lactide) (PEG-PDLLA) micelles (Genexol-PM) for anticancer,[6] and thus the reasons why these micelles are not functioning as expected need to be clarified to advance the therapy in clinic. Once being injected into the blood circulation, the micelles face and interact with the complex biological environment and barriers such as blood components, phagocytosis, and biodistribution before arriving at the lesion site, which may alter their capability to target and transport, thus determining the fate in the body and the final therapeutic efficiency.[7] To develop solutions to address these issues, it is reasonable to Research into the interactions between the micelles and these complex environment and barriers, which mainly dependent on the physical and chemical properties of the micelles,[8] eg, size, charge, stability, and chain conformation.[9–12] For example, positively charged micelles are known to have quite an effect on the blood components, such as platelet activation, coagulation, and hemolysis, resulting in hemocompatibility concerns.[13] And also, it is inevitable that blood protein adsorption occurred when the micelles are injected into the blood steam, forming so called protein corona[14,15] that changes micellar original properties and leads to be specifically recognized by mononuclear phagocytic system (MPS), and finally sequestrated and cleared from the circulation mainly by macrophages in MPS organs such as Kupffer in liver.[16] In addition, the micellar stability plays an important role in delivery efficacy as well since micelles unstable upon being injected when facing blood shear stress would result in release of the loaded drug before reaching the target site.[17] Recently, Fan et al concluded that plasma proteins and blood shear stress affect the stability of the micelles, which directly determines their blood circulation time.[18] Based on the above views, when designing micelles for drug delivering, efforts should be paid to the following aspects: (ⅰ) appropriate effect on the blood components to ensure hemocompatibility, (ⅱ) modulation of protein adsorption to reduce subsequent specific phagocytosis and biodistribution, and (ⅲ) increase of micellar stability in blood and extending their circulation time.

PEGylation is a golden strategy for protecting micelles from protein adsorption and prolonging circulation.[19] Currently clinic approved polymer micelles for patient's cancer therapy including Genexol ® PM and Nanoxel ® M are both shelled with PEG.[20] Traditionally, the protein-repelling property of PEGylation is believed to be related to the molecular structure of the PEG chains, which has the capability to bind water via hydrogen bonds and suppress protein adsorption through steric repulsion mechanism.[21] In recent years, the mechanism of PEG shielding in-depth understanding is found to be dependent on the PEG density and conformation.[22,23] With higher PEG coverage density, the chains tend to form "brush" conformation and thus reducing surface area contacting with proteins. Meanwhile the flexibility of chains and steric repulsion, which is conducive to repelling protein adsorption, are reduced. Conversely, with lower surface PEG density, chains with increasing mobility tend to be close to the inner core and form "mushroom" conformation.[24] Therefore, there may be a balance between the two conformations that achieves optimum protein adsorption resistance.

Herein, we expect to understand these concerns for the clinically relevant PEG-PCL micelles,[25] since they are the best-characterized systems in preclinical research and showing great potential to successfully enter clinical translational in the near future.[26] We hypothesize that the micelles with different surface PEG density and chain conformation would affect their interactions with the blood components, phagocytosis, and biodistribution once injected into the blood, and finally determine their therapeutic efficiency. To address this hypothesis, PCL_n-MPEG micelles that composed of PEG with identical chain length and PCL with tunable chain length (n=20, 30, and 40) were first prepared wherein doxorubicin was encapsulated as a model drug. The surface PEG density and chain conformation were evident by dissipative particle dynamics (DPD) simulation. The effects of micelles on the blood components including red blood cells, platelet, coagulation, and plasma proteins were studied before phagocytosis by macrophages and biodistribution in mice were assayed (Figure 1.). Based on the above results, the relevant mechanisms were proposed and discussed.

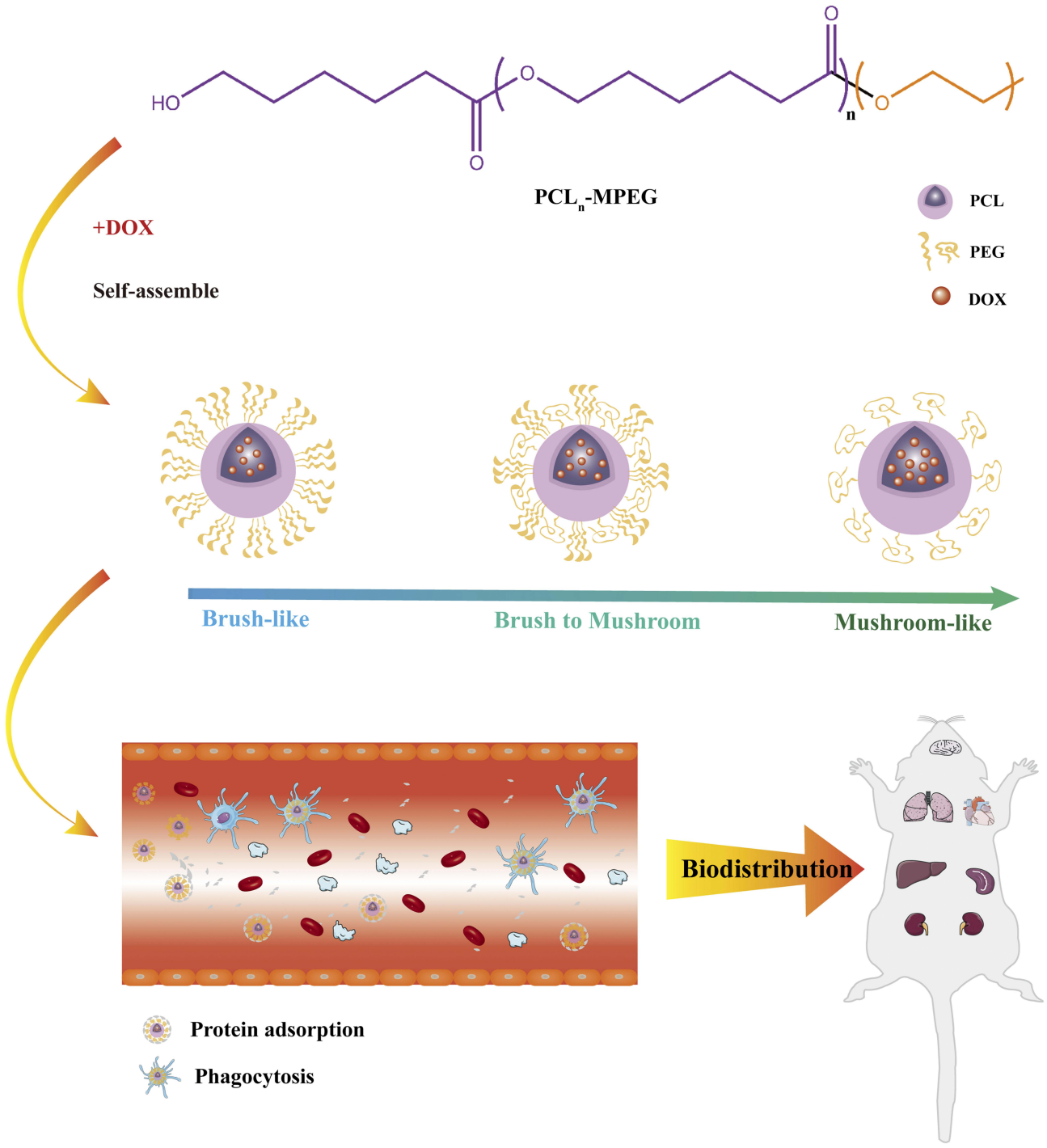

Figure 1 Schematic diagram of co-polymer self-assemble and micellar biodistribution.

Materials and Methods

Materials

ε -Caprolactone (ε -CL) was purchased from Sigma-Aldrich (New Jersey, USA), and was distilled under reduced pressure prior to use. Methoxy polyethylene glycol (MPEG, Mw=1900 Da), doxorubicin hydrochloride (DOX·HCl), fluorescein isothiocyanate (FITC) and heparin sodium were purchased from Aladdin Co., Ltd. (Chengdu, China). 1.1'-dioctadecyl-3,3,3',3'-tetramethylindocarbocyanine (DIL) were obtained from Shanghai Biyuntian Biotechnology Co., Ltd. Anti-CD61-antibody-

fluorescein isothiocyanate (FITC), anti-CD62p-antibody-phycoerythrin (PE) and IgG1 antibody (mouse)-PE, were purchased from BD Pharmingen, BD BioScience Co., Ltd, (San Jose', CA, USA). Blood coagulation including activated partial thromboplastin time (APTT), prothrombin time (PT), thrombin time (TT), and fibrinogen (Fib) reagents were purchased from SIEMENS Ltd.

Synthesis of PCL-MPEG Copolymers

The PCL_n-MPEG copolymer was synthesized by ring-opening polymerization of ε-caprolactone using MPEG (Mw=1900) as the initiator as previous report.[27] ^{1}H-NMR spectra were recorded on a 400M Bruker NMR Spectrometer (400 MHz) at 25 °C to determine the chemical structure of the copolymers in chloroform-d ($CDCl_3$). 10 mg of each sample was dissolved in 0.5 mL of solvent.

Preparation and Characterization of Micelles

To mimic the practical application condition, the DOX-loaded micelles were prepared by a dialysis method. First, 40 mg DOX·HCl was neutralized by 40 uL TEA in 10 mL mixed solvent of MeOH and DMSO (v/v =1:1) and then the 200 mg copolymer was added into the solution. When the copolymer was completely dissolved, the solution was injected into ultra-purified water at a rate of 200μL/min and stirred for 6 h, after which the solution was transferred to a dialysis bag (MWCO 1000) and dialyzed against deionized water at 4 °C for 48 h. The final concentration of the micelle was adjusted to 10 mg/mL and the solution was stored at 4 °C for next use. The drug loading content (DLC) of the micelle was measured by ultraviolet spectroscopy at 483 nm and calculated by the equation (1):

$$\boldsymbol{DLC(\%) = \frac{amount\ of\ drug\ in\ micelle}{amount\ of\ drug\ loaded\ micelle} \times 100(\%)} \quad (1)$$

Dynamic light scattering (DLS) (Malvern Zetasizer Nano-ZS 90, UK) was used to determine the size, zeta potential, and polymer dispersity index (PDI) of the micelles (water solution, pH=7.0). Transmission electron microscopy (TEM) (HT7700, Hitachi, Japan) was employed to observe the morphology of the micelles. For specimen preparation, 50μL of micellar solution was dropped onto a copper grid, and then stained with phosphotungstic acid (1wt %) for 1 minute and dried with filter paper.

Dissipative Particle Dynamics Simulation

A mesoscale meshless particle simulation algorithm, dissipative particle dynamics (DPD), was used for simulating complex hydrodynamic behavior. The simulations were executed with the DPD module in the software Materials Studio 5.0 from Accelrys Software Inc., USA. The computer model was DELL PowerEdge SC430.

With a coarse-grained module, DPD simulation represented whole molecule or multi-molecules as single bead, which were governed dynamically by:

$$\frac{d\vec{v_i}}{dt} = \frac{\vec{F_I}}{m_i} \quad (2)$$

$$\frac{d\vec{r_i}}{dt} = \vec{v_i} \quad (3)$$

Where $\vec{v_i}$, $\vec{r_i}$, $\vec{f_i}$ and m_i represent the vector of velocity, position, force and mass of the *i*th bead, respectively. The force between *i*th and its neighbor bead *j* is the sum of conservative force (F_{ij}^C) dissipative force (F_{ij}^D) and random force (F_{ij}^R):

$$f_i = \sum_{i \neq j}(F_{ij}^C + F_{ij}^D + F_{ij}^R) \quad (4)$$

There is cutoff radius (r_c) for reducing calculation time. Only when the distance between beads *i* and *j* less than r_c, the interaction force between two beads is calculated. The conservative force is soft repulsion force between beads *i* and *j*:

$$F_{ij}^{C} = a_{ij}\left(1 - \frac{r_{ij}}{r_c}\right)\widehat{r_{ij}} \tag{5}$$

where a_{ij} is the interaction strength between two beads and is related to the Flory-Huggins (X_{ij}).

$$a_{ij} = a_{ii} + 3.27X_{ij} \tag{6}$$

$$X_{ij} = \frac{\Delta E_{mix} V_r}{RT\varphi_i\varphi_j V} \tag{7}$$

Where T is temperature and R is the gas constant. $\varphi_i$and $\varphi_j$refer to the volume fractions of beads i and j. V represents total volume and V_r is reference volume.

The value of random force and dissipative force are related by the theorem of Fluctuation-dissipation, and its statistic value is in line with the system temperature.

$$F_{ij}^{D} = -\frac{\sigma^2\left(w\left(r_{ij}\right)\right)^2}{2KT}\left(\widehat{r_{ij}} \cdot V_{ij}\right)\widehat{r_{ij}} \tag{8}$$

$$F_{ij}^{R} = -\frac{\sigma_\omega\left(r_{ij}\right)\widehat{r_{ij}\zeta}}{\sqrt{\delta_t}} \tag{9}$$

Where K is Boltzmann constant. T mean the system temperature, σ represent the noise strength which control the random force, ζ denote a Gaussian random number with zero mean and unit variance, δ_t represent simulation time step.

Micellar Stability

A simple straight microchannel was made out of infusion hose according to Sun's study.[28] The microchannel was connected to a 1 mL syringe. The PCL_n-MPEG micelle was loaded in the syringe and fixed on a syringe pump (Model R452, RWD Life Science Co., Ltd, Shenzhen, China.), and the parameters were set to: Volume 1 mL, Diameter 4 mm, Mode continuous (Infusion/Withdraw). The solution passed from the microchannel and repeated five cycles. The micelle solution after subjected to shear was collected. Nanoparticle tracking analysis (NTA) (Zetaview, Particle Metrix, Germany) was used to detect concentration of micelles before and after subjected to shear. Measurements were performed under following settings: Shutter: 70; Scattering Intensity: 4.0; Temperature: 25 ºC. The analysis version was ZetaView Software 8.05.11 with parameters: Minimum size: 5 nm. Maximum size: 1000 nm. Minimum brightness: 20. Laser wavelength: 488 nm.

Blood Collection

Both whole blood and fresh frozen plasma (FFP) from three healthy donors were anticoagulated with sodium citrate. The anticoagulated whole blood was respectively centrifuged at 3000 g for 10 minutes to obtain plasma and centrifuged at 180 g for 15 minutes to obtain platelet-rich plasma (PRP). Red blood cell (RBC) suspension was obtained by washing anticoagulated whole blood with normal saline for three times and adjusting hematocrit (HCT) to 10%. All the experiments involved blood components were approved by Ethical Committee of Institute of Blood Transfusion, Chinese Academy of Medical Sciences & Peking Union Medical College. The blood donors had written informed consents for the use of their blood samples in accordance with the Declaration of Helsinki.

The Effect on Blood Components

Red Blood Cells

Hemolysis

The hemolysis induced by the micelles was evaluated by ortho-tolidine method. RBCs suspension (10% hematocrit) (270μL) was mixed with micelle solution (30μL) and incubated at 37 ºC for 1 h. Then the mixture was centrifuged at 1,500 g for 5 min to obtain the supernatant for hemoglobin concentration analysis according to previous report.[28] In brief, 20μL of supernatant was added to1 mL of ortho-tolidine solution (0.2 g/ 60 mL acetic acid) and 1 mL of hydrogen

peroxide (1 g/ L) for 10 min incubation. Following, 10 mL of acetic acid (10%) was added to stop the reaction. The free hemoglobin content was determined by the absorbance at a wavelength of 435 nm. A standard hemoglobin solution with concentration of 100 mg/L was used as a standard control and diluted water (DW) was used as a hemolysis control. The hemolysis was calculated by the following equation.

$$\boldsymbol{Hemolysis(\%) = \frac{A_1}{A_0} \times \frac{100 - Hct(\%)}{Hb(g/l) \times 1000} \times 100\%} \quad (10)$$

where A_1 means the absorbance of sample. A_0 means the absorbance of standard sample. Hct means hematocrit. Hb means the hemoglobin concentration of RBC suspension.

Aggregation

30μL of micelle solution was added to 270μL of anticoagulated whole blood incubating at 37 ºC for 1h, and then the mixture was centrifuged at 1000 g for 3 minutes at 4 ºC. The supernatant (40μL) was mixed with RBCs sediment (3μL) and examined by an Olympus CKX 43 optical microscopy. Positive and negative controls were respectively prepared by replacing micelle with polyetherimide (PEI) and normal saline (NS).

Coagulation

60μL of micelle solution was mixed with 540μL of FFP and then incubated at 37 ºC for 1h, after which the mixture was centrifuged at 2500 rpm for 10 minutes at 4 ºC to collect supernatant. Four coagulation assays were carried out, eg, APTT, PT, TT, and Fib, using an automated coagulation analyzer (Instrumentation Laboratory ACL ELITE, USA). Heparin (HP, 0.75 IU/mL) was used as a positive control, while NS was used as a normal control.

Platelet Activation

Platelet activation was assayed according to previous reports. In brief, micelle solution (30μL) was added to PRP (270μL) and incubated at 37 ºC for 1 h. The expression of the CD62p was detected in 10,000 total events counted using a flow cytometry (Becton-Dickinson, San Jose, CA, USA). PRP incubation with thrombin (10 IU/mL) and NS were used as positive and negative control, respectively.

Protein Adsorption

BSA, fibrinogen, and plasma were used as model proteins for adsorption assays. In brief, 700μL of micelle (10 mg/mL) was mixed with 200μL of BSA (2 mg/mL), fibrinogen or fresh plasma and incubated in a 37 ºC water bath for 2 h. The resulting solution was centrifuged at 18,000 rpm for 30 minutes at 4 ºC. The precipitate was washed with 400 μL PBS for three times, and then incubated with 400μL of sodium dodecyl sulfate (SDS) 2% (W/V) at 37°C for 1 h. Finally, the supernatant was obtained by centrifugation at 18,000 rpm at 4 ºC for 30 minutes. The protein adsorption was determined by Pierce BCA Protein Assay Kit and Micro BCA Protein Assay Kit.

Phagocytosis by Macrophage

Cell Culture

RAW264.7, a murine macrophage cell line, was cultured in Dulbecco's Modified Eagle's Medium (DMEM) supplemented with 10% fetal bovine serum, 50 U/mL penicillin G, and 50 U/mL streptomycin at 37 ºC using a humidified 5% CO_2 incubator. The cells in their three passages were used for the following experiments.

Laser Scanning Confocal Microscope

The phagocytosis of micelles by RAW264.7 cells was first assayed by laser scanning confocal microscopy (LSCM). In brief, RAW264.7 cells were cultured in a dish with a glass bottom at a density of 1×10^6/cells in a 37 ºC, 5% CO_2 incubator. After 24 h the medium was removed and the dish was washed twice with 0.01 M PBS before micellar solution that was diluted to 10μg/mL with DMEM was added to the dish. After continuing to incubate for 4 h, the micellar solution was removed and the dish was washed three times with cold 0.01 M PBS. Finally, the phagocytosis of the micelles was observed using a laser confocal microscope (Nikon A1R + MP, Japan).

Flow Cytometry

The phagocytosis of micelles by RAW264.7 was further quantified by flow cytometry. In brief, the cells were seeded in a 6-well plate at a density of 1×10^5/mL in a 37°C, 5% CO_2 incubator. After cultured for 24 h, the medium was removed and the plate was washed with cold 0.01 M PBS, and then 200μL of FITC-labeled micelle that was diluted to 10μg/mL with DMEM was added to each well of the plate. After continuing to incubate for 4 h, the culture medium was removed and the plate was washed two times with cold 0.01 M PBS, and the cells were collected by pipetting thereafter. The obtained cells were centrifuged at 1000 rpm for 5 minutes to remove the supernatant, and then the cells were resuspended in 1 mL of PBS. After three times of this centrifugation-resuspension process, the cells were resuspended in 300μL PBS. Finally, 10, 000 cells were collected for each sample by flow cytometry, and the phagocytosis was quantified by mean fluorescence intensity (MFI).

In vivo Biodistribution

Animal experiments were performed in accordance with the Chinese National Guidelines for the Use and Care of Experimental Animals, approved by the Animal Ethical Committee of West China Hospital, Sichuan University (NO. 20211306A). The in vivo biodistribution of PCL_n-MPEG was investigated in Kunming mice (Dashuo Laboratory Animal Co. Ltd., Chengdu, China) by fluorescence optical image approach using IVIS SPECTRUM (PerkinElmer, USA). All animals were housed in Animal Center of West China Hospital and fed a standard rodent diet ad libitum with 24-h access to water while kept on a 12-hour light-dark cycle at temperature 24 ºC and humidity 55 ± 5%. 24 mice acclimatized at least for 4 days prior to the experiments. Dir fluorescently labeled PCL_n-MPEG micelles with different DP of PCL in 100μL normal saline were injected intravenously into Kunming mice via tail vein, respectively (n=3). The same volume of normal saline without micelles was administrated as blank control (n=3). All animals were euthanized by CO_2 overdose at 1h and 24 h after injection, respectively. Major organs (liver, lungs, spleen, kidneys, brain and heart) were excised and imaged using the IVIS Spectrum with an excitation bandpass filter at 710 nm and an emission at 780 nm. The fluorescence intensities were determined by the Living Imaging software using operator-defined regions of interest (ROI) measurements on organs.

Statistics Analysis

All data were presented as the mean ± standard deviation (SD). Statistical analysis was performed with SPSS 17.0 and analysis of variance (ANOVA) was used for evaluating statistical significance. The probability value $p < 0.05$ was considered a significant difference. Statistical significance: "*", $p < 0.05$; "**", $p < 0.01$; "***", $p < 0.005$, "****", $p < 0.0001$, and "ns", no significance.

Results and Discussion

Characterization of Copolymers and Micelles

The copolymer PCL-MPEG was characterized by ^{1}H-NMR and the structure was shown in Figure 2. The characteristic peaks assigned to the MPEG block were confirmed (-$OCH_2CH_2OCH_3$, δ 3.36; -$OCH_2CH_2OCH_3$, δ 3.63; -$OCH_2CH_2OCH_3$, δ 4.04;), and also the characteristic peaks attributed to PCL block were ascertained (-$COOCH_2CH_2CH_2CH_2CH_2$-, δ 2.29; -$COOCH_2CH_2CH_2CH_2CH_2$-, δ 1.64; -$COOCH_2CH_2CH_2CH_2CH_2$-, δ 1.37; -$COOCH_2CH_2CH_2CH_2CH_2$-, δ 4.04;). The unit number of PCL block was calculated as 20, 30, and 40, respectively, by comparing the integral ratio of the proton signals in the ^{1}H-NMR spectra.

The particle size, surface charge and distribution of the micelles were determined by DLS. As shown in Table 1, all the micelles were negatively charged, and the hydrodynamic average diameter was in the range of 40–60 nm with narrow PDI. TEM (Figure 3) showed that the micelles exhibited spherical morphology, with a diameter about 30 nm. The size of the micelles determined by TEM was smaller than that in DLS determination because TEM operation in the dry state while DLS operation in the wet state. The ratio of PEG/PCL was reduced with the increasing of PCL chain length. Low solubility drugs such as DOX could be physically encapsulated into micelles via hydrophobic interactions with hydrophobic segments.[29] Drug loading content (DLC) increased with the length of PCL resulted

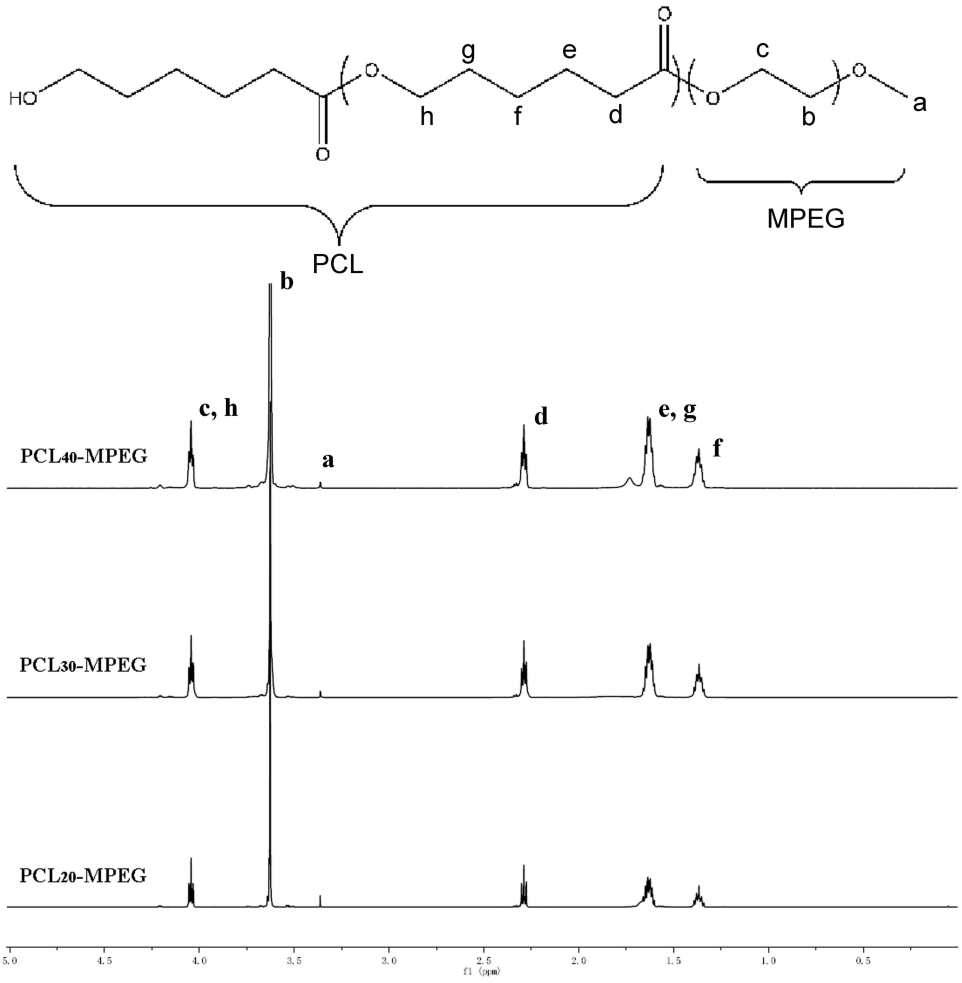

Figure 2 The ^{1}H-NMR spectra of the copolymers.

from the strengthen hydrophobic interactions in the micellar core. The difference of all micellar size was not significant.

DPD Simulation

For deeply understand the influence of PCL chain length on the surface PEG density and conformation, dissipative particle dynamics (DPD) simulations were employed. The coarse grain models comprising of PCL-MPEG and DOX were shown in Figure S1. The molecular structure of DOX was divided into one DOX1 bead (colour: brown), one DOX2

Table 1 The Characteristics of PCL_n-MPEG Micelles

Micelles	Diameter (nm)	Zeta Potential (mv)	PDI	PEG/PCL	DLC (%)	Peak of RDF
PCL_{20}-MPEG	40.52±0.58	−8.97±0.16	0.28±0.02	0.8	4.45	1
PCL_{30}-MPEG	60.79±0.32	−13.5±1.01	0.29±0.02	0.6	9.24	0.95
PCL_{40}-MPEG	51.56±0.91	−0.45±0.04	0.28±0.02	0.4	12.6	0.39

Abbreviations: MPEG, methoxy polyethylene glycol; PCL, poly(ε-caprolactone); DOX, doxorubicin; DOX·HCl, doxorubicin hydrochloride; DLS, dynamic light scattering; TEM, transmission electron microscopy; DPD, dissipative particle dynamics; NTA, nanoparticle tracking analysis; DLC, drug loading content; PSA, poly (salicylic acid); NPs, nanoparticles; PEG-PDLLA, polyethylene glycol-poly (D,L-lactide); MPS, mononuclear phagocytic system; FITC, fluorescein isothiocyanate; DIL, 1.1'-dioctadecyl-3,3,3',3'-tetramethylindocarbocyanine; PE, phycoerythrin; $CDCl_3$, chloroform-d; FFP, fresh frozen plasma; PRP, platelet-rich plasma; RBC, Red blood cell; HCT, hematocrit; DW, diluted water; PEI, polyetherimide; NS, normal saline; APTT, activated partial thromboplastin time; PT, prothrombin time; TT, thrombin time; Fib, fibrinogen; HP, Heparin; SDS, sodium dodecyl sulfate; DMEM, Dulbecco's Modified Eagle's Medium; LSCM, laser scanning confocal microscopy; MFI, mean fluorescence intensity; ROI, regions of interest; SD, standard deviation; ANOVA, analysis of variance; RDF, radial distribution functions; EPR, enhanced permeability and retention; RES, reticuloendothelial system.

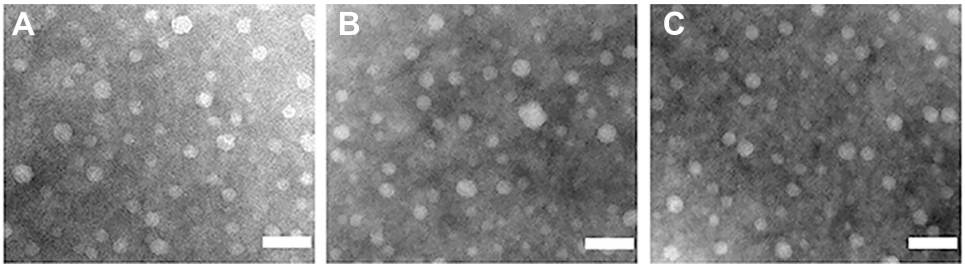

Figure 3 The TEM images of PCL_{20}-MPEG (**A**), PCL_{30}-MPEG (**B**), PCL_{40}-MPEG (**C**) micelles, respectively. The scale bar is 100nm.

bead (colour: light blue), and one DOX3 bead (colour: dark blue). The polymer PCL-MPEG was segmented into PEG (colour: green), PCL (colour: red). A WATER bead contained about six molecules. For better visualization, the WATER beads were all hidden in the figures below. Referred to Yang's research,[27] the bead density was 3.0.

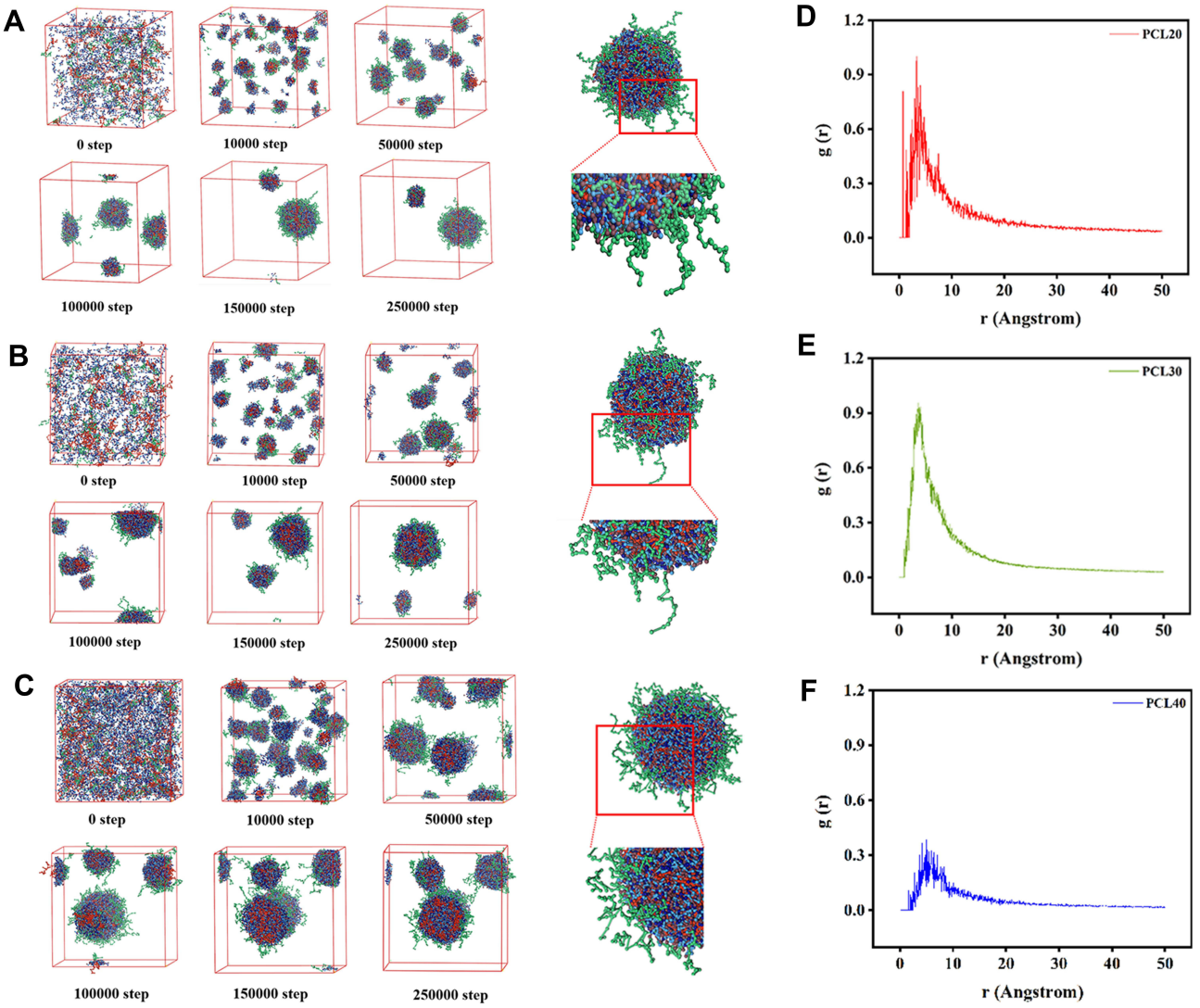

Figure 4 (**A–C**) The micellar self-assembled state at different simulation time and locally enlarged images of conformation. (**D–F**) The normalized RDF curves of the three micelles.

The average volume of the beads was about 210 Å3. A box size of 30 nm× 30 nm× 30 nm with periodic boundary condition was used. Simulation steps of 250,000 were applied and time steps were 0.05 ns. The a_{ij}, interaction parameters, were calculated according to equations (7,8) and were shown in supporting information Table S1.

It could be seen from the Figure 4., the self-assembly process of three micelles with different PCL chain lengths tended to be equilibrium during the steps of 150,000–250,000. The micellar simulation figures at steps 250,000 were chosen. It could be seen intuitively that the PEG bead chains (colour: green) of PCL_{20}-MPEG (Figure 4. A) were generally extended outward. In PCL_{40}-MPEG (Figure 4. C), the PEG bead chains were relatively curly and the end was close to the core of micelles. The bead chains of PCL_{30}-MPEG (Figure 4. B) were both stretched outward and curled to the inner core. In addition, according to radial distribution functions (RDF) curves, that was, the probability that the same beads within the certain distance range, the aggregation degree of PEG beads on the surface might be objectively inferred.[30,31] Within the same distance range, the peak of aggregation of PEG beads in PCL_{20}-MPEG micelle (Figure 4. D) appeared the earliest and was the highest (1.0). Followed by PCL_{30}-MPEG (Figure 4. E) (0.95), and the lowest was PCL_{40}-MPEG (Figure 4. F) (0.39). It might be considered that among three micelles, the highest degree of surface PEG coverage was PCL_{20}-MPEG, the lowest was PCL_{40}-MPEG, and the degree of PCL_{30}-MPEG lied between the above two.

DPD simulation provided a new perspective for objectively understanding how surface density and conformation change with PCL chain length. In the present study, the PEG density on micellar surface decreased with the increase of PCL chain length. A previous study on the effect of PEG density on nanoparticles by Du et al also pointed out that PEG density gradually declined as the molecular weight of PCL increased.[32] From the meaning of the RDF curve, it was not difficult for us to understand that when the density of PEG was higher within a certain surface range, the mobility of the chain would decrease and it was more inclined to extend outward. On the contrary, when the density was lower, the chain had more space to move or curl. These two situations led to different conformations of the PEG chain that named as "brush" and "mushroom"[24,33] as the DPD simulation shown.

Micellar Stability

The prerequisite for the micellar delivery system to achieve the expected targeting and high efficacy is that the micelle can still maintain the integrity after being injected into the blood and suffering variable physiological barriers, and release the payloads at target site to realize the treatment of lesions.[34] According to the research of Shen et al, upon being injected into blood, in addition to the fact that protein adsorption affected micellar properties, the shear stress in blood microchannel also participated in affecting micellar stability and led to premature release of payloads.[25] Therefore, stability needs to be taken into consideration when designing micelles for drug delivery through intravenous injection.

Syringe pump with a connected microchannel simulated the blood microchannel and micellar solutions were through it five cycles with a mode of continuously infusion/withdraw to mimic shear stress in blood circulation. Nanoparticle tracking analysis (NTA), which could calculate the hydrodynamic diameter and concentration of nanoparticles, was used to detect the concentration of micelles before and after shear stress. Real-time image of NTA detecting micelles was shown in Figure 5. It could be seen that the fluorescence of particles after five cycles (D-F) were reduced to a certain extent compared with those before untreated (A-C). The statistic results shown in Figure 5. G. demonstrated that among three groups of micelles after shearing, the reduced concentration of intact micelles in descending order was PCL_{20}-MPEG, PCL_{30}-MPEG and PCL_{40}-MPEG. It might indicate that PCL_{40}-MPEG kept more intact when suffered shear stress in circulation. From the perspective of the micellar design, the micelles showed increasing stability as the chain length of PCL increased when subjected to shearing force, which may attribute to longer PCL chains, higher crystallization and more stability of micelles.[35]

Red Blood Cells

The mature periphery RBCs are biconcave cells with negative charged surface. Various extraneous substances may have different effects on RBCs and change their form and physiological function. Hemolysis is a vital and essential parameter for biomaterial evaluation that once happening can lead to fatal complications such as acute renal failure and shock. All the three micelles presented no evident hemolysis as shown in Figure 6. A and B. The hemolysis percentage (0.86

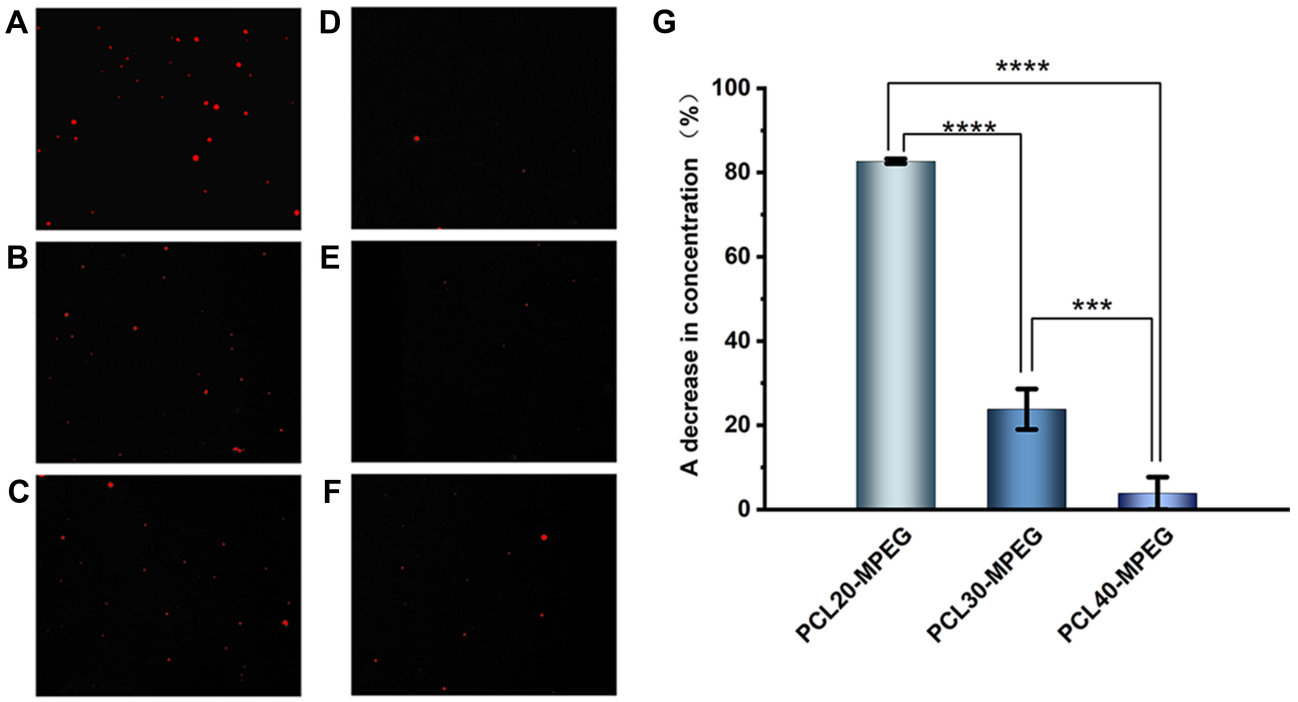

Figure 5 The images of the NTA for the micelles (the red florescence represent micelles). (**A–C**) Micelles before shear stress. (**D–F**) Micelles after shear stress. (**G**) The decrease in concentration of micelles after shear stress. (n=3, ***p <0.005, ****p <0.0001).

±0.31%, 0.85±0.23%, 0.88±0.25% for PCL_{20}-MPEG, PCL_{30}-MPEG and PCL_{40}-MPEG, respectively) were far below 5% considered as low risk of hemolysis according to ISO10993-5 and ISO10993-4.[36]

Normal red blood cells in the circulation are in a dynamic balance between aggregation and dispersion and every cell maintains a relatively individual status to each via electrostatic interaction. RBCs aggregation partly determines the viscosity of blood meaning that irreversible aggregation may cause micro thrombosis leading to microcirculation disorder and anoxia.[37] As shown in Figure 6. C, RBCs presented a normal distribution with typical biconcave shape in all three groups, which was same to NS group. Possessing negative charge on their membrane surface, RBCs were easily influenced by positive charged materials such as PEI. When reacted with positive charged matters, the electrostatic balance of RBC membrane was destroyed resulting in irreversible aggregation and various degrees of hemolysis. In this work, the PCL_n-MPEG micelles were negatively charged. Combing with no aggregation and low risk of hemolysis, these micelles demonstrated good compatibility with RBCs.

Coagulation

Coagulation is also an essential aspect for biomaterial evaluation, for that pro-coagulation and anti-coagulation, these two extreme situations, sometimes mean thrombosis or bleeding are both harmful to body. Interaction with factors along the coagulation pathway sometimes leads to coagulation dysfunction. As for intrinsic and extrinsic coagulation pathway,[38] APTT and PT are two common parameters respectively. Moreover, TT reflects the time during thrombin triggers the conversion of fibrinogen to fibrin. Another important parameter is the concentration of fibrinogen, a protein that plays a key role in thrombosis and homeostasis. According to previous report,[27] when the extended time of APTT is greater than 10s or PT/TT is greater than 3 s, the haemostatic function of human body is disturbed. In our study, APTT, PT, TT and Fib of the micelles in all three groups were within the standard range the same to NS group (Figure 7.). Heparin was used as positive control that prolonged APTT (>150 s), PT (33.5 ±1.3 s) and TT (>40 s).

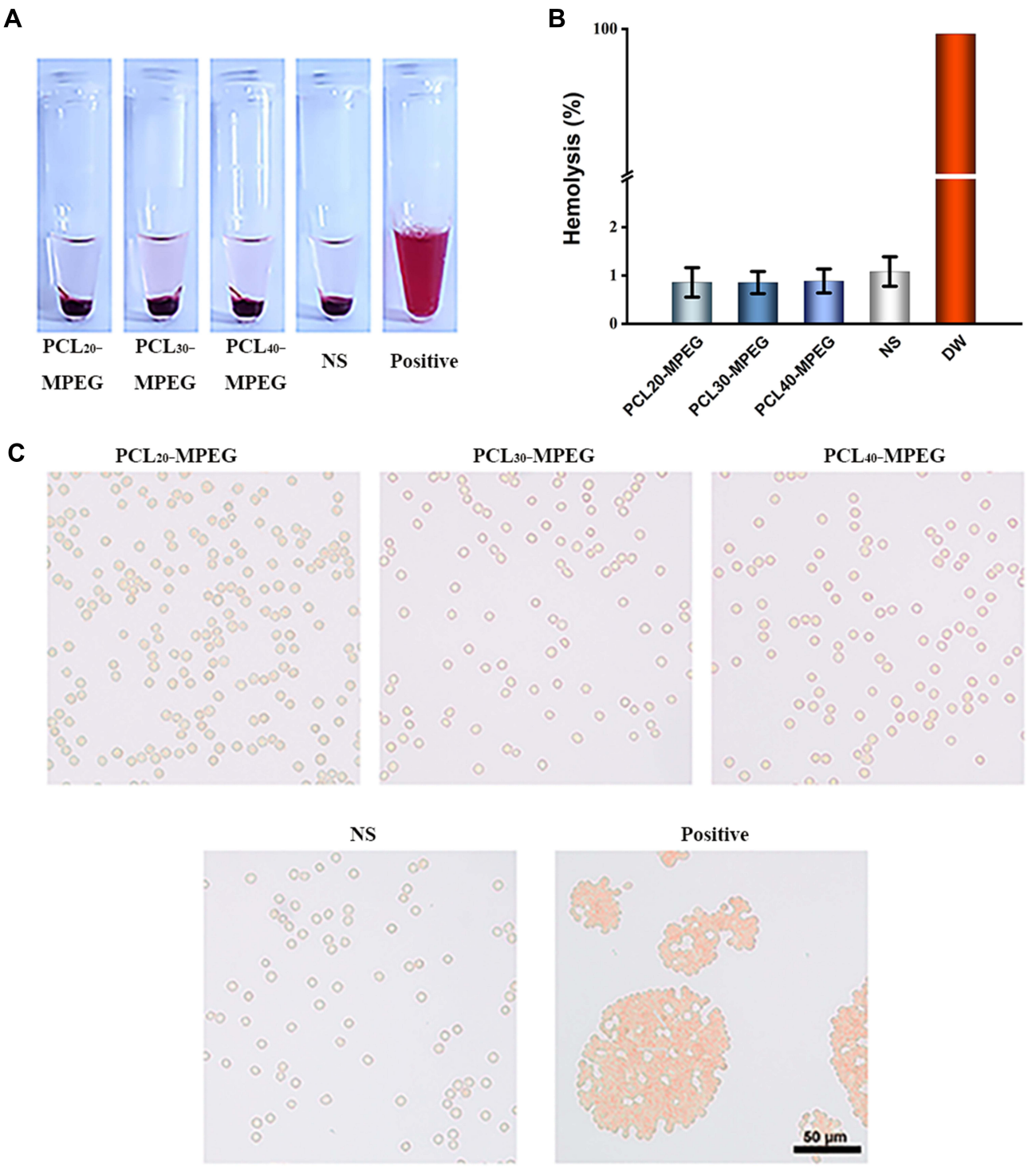

Figure 6 (**A**) The appearance of the micelles incubated with red blood cells suspension. (**B**) The hemolysis ratio of the micelles incubated with red blood cells suspension (n=3). (**C**) The images of the red blood cells aggregation induced by the micelles, NS, and Positive (PEI). The scale bar is 50um.

Platelet Activation

Platelets are activated when they contact injured endothelium or some surface of extraneous materials and then these platelets secret α-granules and expressed P-selectin (CD-62P), which plays a significant role in platelet adherence, on their membrane.[39] Thus, we used the marker anti-CD62P to label the activated platelets and flow cytometry was performed, as shown in Figure 8. A and B. The results showed that the percentages of activated platelets in PCL_n-

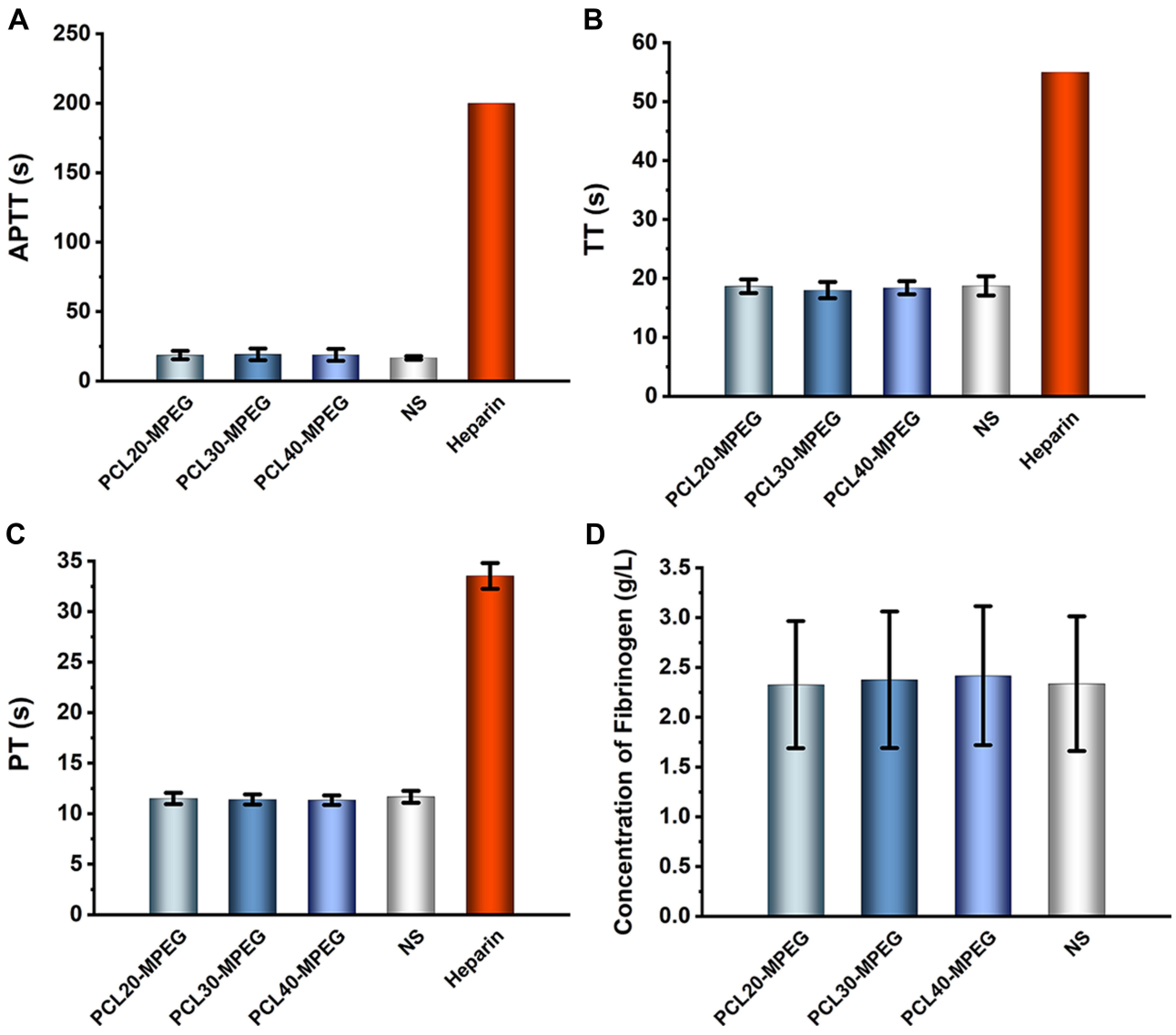

Figure 7 The effects of the micelles on blood coagulation. (**A**) APTT (**B**) TT (**C**) PT and (**D**) Fibrinogen. (n=3).

MPEG groups were all at a low level (2.35 ±0.50%, 2.90 ±0.14%, 2.60 ±0.28% corresponding to PCL_{20}-MPEG, PCL_{30}-MPEG and PCL_{40}-MPEG, respectively) demonstrated that the material did not induce platelet activation. Previous study[27] reported that materials with positive charged surface easily to activate platelet and induce platelet aggregation. In our study, these micelles with negative charge showed a good compatibility with platelet.

Protein Adsorption

The blood proteins rapidly adsorbed onto micellar surface when micelles were intravenous injected into the body, and then formed "protein corona"[14] in a manner that dependent on the physical and chemical properties of the micelles, which changed micellar initial properties and produced new "biological identity",[40] and thus influenced recognition and clearance from the mononuclear phagocytic system (MPS).[21] Considered that the immune proteins play a vital role in mediating the following phagocytosis, the two proteins, eg, albumin and fibrinogen, were selected to study the micellar protein adsorption. As shown in Figure 9. A, the BSA adsorption on micelles was 19.61±0.90, 11.44 ±0.27, and 15.12 ±0.12μg/mL for PCL_{20}-MPEG, PCL_{30}-MPEG and PCL_{40}-MPEG, respectively, indicated that the adsorption amount was first decrease and then increase with the increase of the PCL chain, in which the PCL_{30}-MPEG had the lowest adsorption

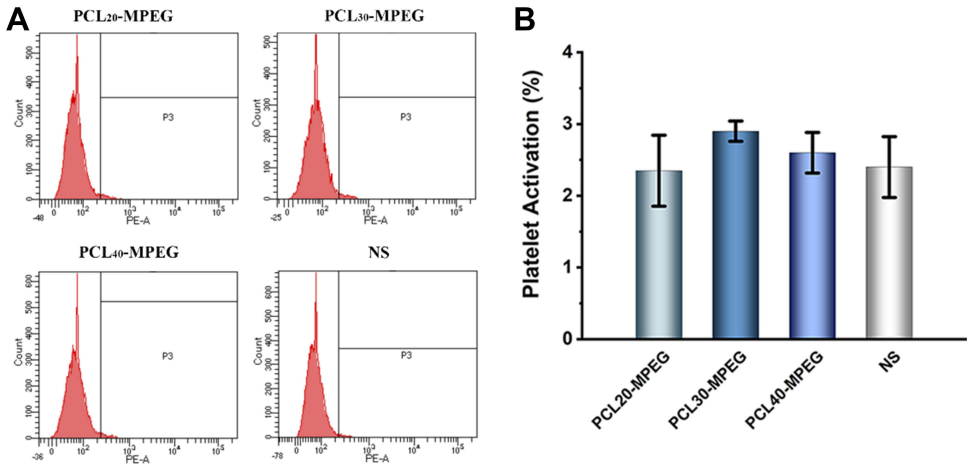

Figure 8 The effects of micelles on platelet activation. (**A**) Flow cytometry analysis of platelet activation. (**B**) The percentages of CD-62P that represent platelet activation. The PRP was incubated with micelles and controls. The expression of CD62p was determined using anti-CD62p antibody (n=3).

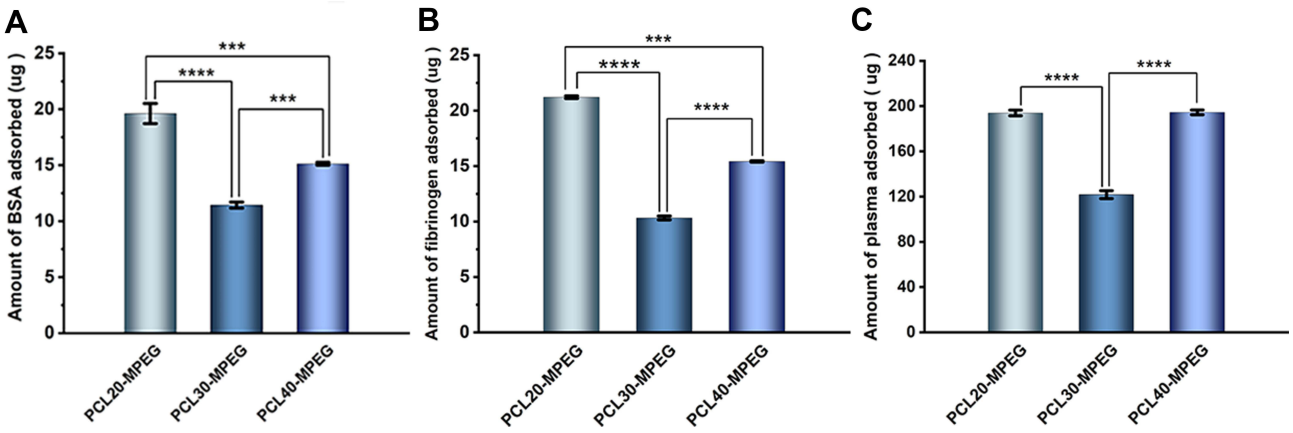

Figure 9 The amount of protein adsorption on the micelles. (**A**) BSA adsorption. (**B**) Fibrinogen adsorption. (**C**) Human plasma protein adsorption. (n=3, ***p<0.005, ****p <0.0001).

of BSA, with PCL_{40}-MPEG followed and PCL_{20}-MPEG was the highest. The adsorption of fibrinogen was similar to that of BSA, and PCL_{30}-MPEG remained the lowest one (Figure 9. B). To mimic blood environment, plasma that contains much more complex proteins than single BSA or fibrinogen was used to further observe the protein adsorption on the micelles. As shown in Figure 9. C, the plasma protein adsorption increased nearly ten-fold than that incubated with BSA and fibrinogen alone since there were more types and amounts of proteins in plasma, and also the similar trend was investigated that the adsorption of plasma protein on the PCL_{30}-MPEG micelle was significantly lower than that of PCL_{20}-MPEG and PCL_{40}-MPEG micelles.

Phagocytosis by Macrophage

When micelles were injected into the blood stream, the non-specific immune reactions were simultaneously activated, in which the macrophage phagocytosis played a critical role in immune defense to clear the micelles from the blood.[41,42] The macrophage phagocytosis was therefore significantly determined the fate of the micelles before arriving at the lesion site. In our study, the macrophage was respectively cultured with plasma free micelles (plasma- group) and plasma-incubated micelles (plasma+ group) to investigate the phagocytosis. As shown in Figure 10. A, the red fluorescence demonstrated the phagocytosis of three micelles by macrophage in both two groups. The mean fluorescence intensity (MFI) denoted the quantification of phagocytosis of the micelles using flow cytometry (Figure 10. B, C, and D). In

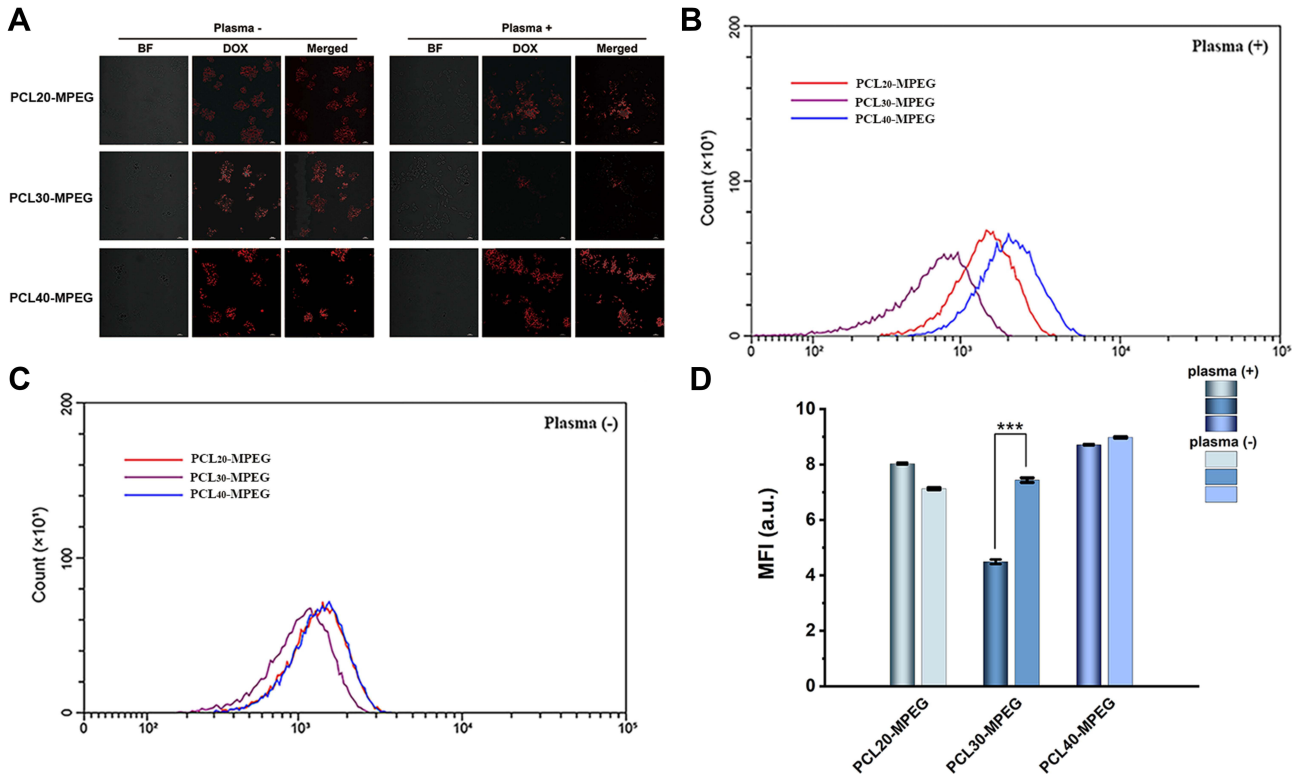

Figure 10 (**A**) The confocal images of the phagocytosis of the micelles by RAW264.7. The scale bar is 20um. (**B** and **C**) The flow cytometry results of the phagocytosis of the micelles by RAW264.7. (**D**) The quantification of the phagocytosis of micelles by mean fluorescence intensity (MFI). (n=3, ***p <0.005).

plasma- group, the PCL_{20}-MPEG, PCL_{30}-MPEG and PCL_{40}-MPEG had MFI of 7.13, 7.43, and 8.98, respectively, indicated that the PCL_{40}-MPEG has the highest phagocytosis amount by macrophage. Interestingly, in plasma+ group that the micelles incubated with plasma prior to culture with macrophage, the phagocytosis of PCL_{30}-MPEG was dramatically decreased and the MFI was the lowest among all micelles, while the MFI of other two micelles had little change after plasma incubated. In general, protein adsorption on micelles after plasma incubation plays a role in de-opsonization thus evades recognition and phagocytosis by macrophages.[43] Attractively, in our study, with plasma incubation, the lowest phagocytosis of PCL_{30}-MPEG among all micelles was consistently with the result of protein adsorption on micellar surface in plasma that was PCL_{30}-MPEG significantly lower than that of PCL_{20}-MPEG and PCL_{40} -MPEG, which most likely resulted from the PEG coverage and conformation of PCL_{30}-MPEG micelles.

In vivo Biodistribution

The highly effective treatment capability of micelles for drug delivery primarily relies on their targeting accumulation at lesion site[2] and is capable of benefiting from various targeting strategies such as stimulus responsive,[44] acceptor-ligand mediation[45] or enhanced permeability and retention (EPR) effect in cancer,[46] however, the therapeutic efficacy is remains challenged by the fact that the majority of micelles are rapidly accumulated in the organs of the reticuloendothelial system (RES) and removed from the blood after intravenous injection, subsequently leading to low concentration to the lesion site. For example, Bae et al summarized that more than 95% of the nanoparticles injected accumulated in other organs, particularly in liver, lungs, and spleen.[47] Thus, the biodistribution of the micelles determines whether its payload could accumulate in the target site. In this work, a fluorescence in vivo optical imaging approach was used to investigate the biodistribution of the three PCL_n-MPEG micelles in main organs of mice. The organs included liver, spleen, lung, heart, brain and kidney were harvested respectively at 1 hour and 24 hours since the micelles injected into the mice tail vein. As shown in Figure 11, at both 1 and 24h time points, there was almost no fluorescence in brain, heart, and kidney, indicated that PCL_n-MPEG micelles did not pass through the blood-brain barrier taken up by brain and not accumulated

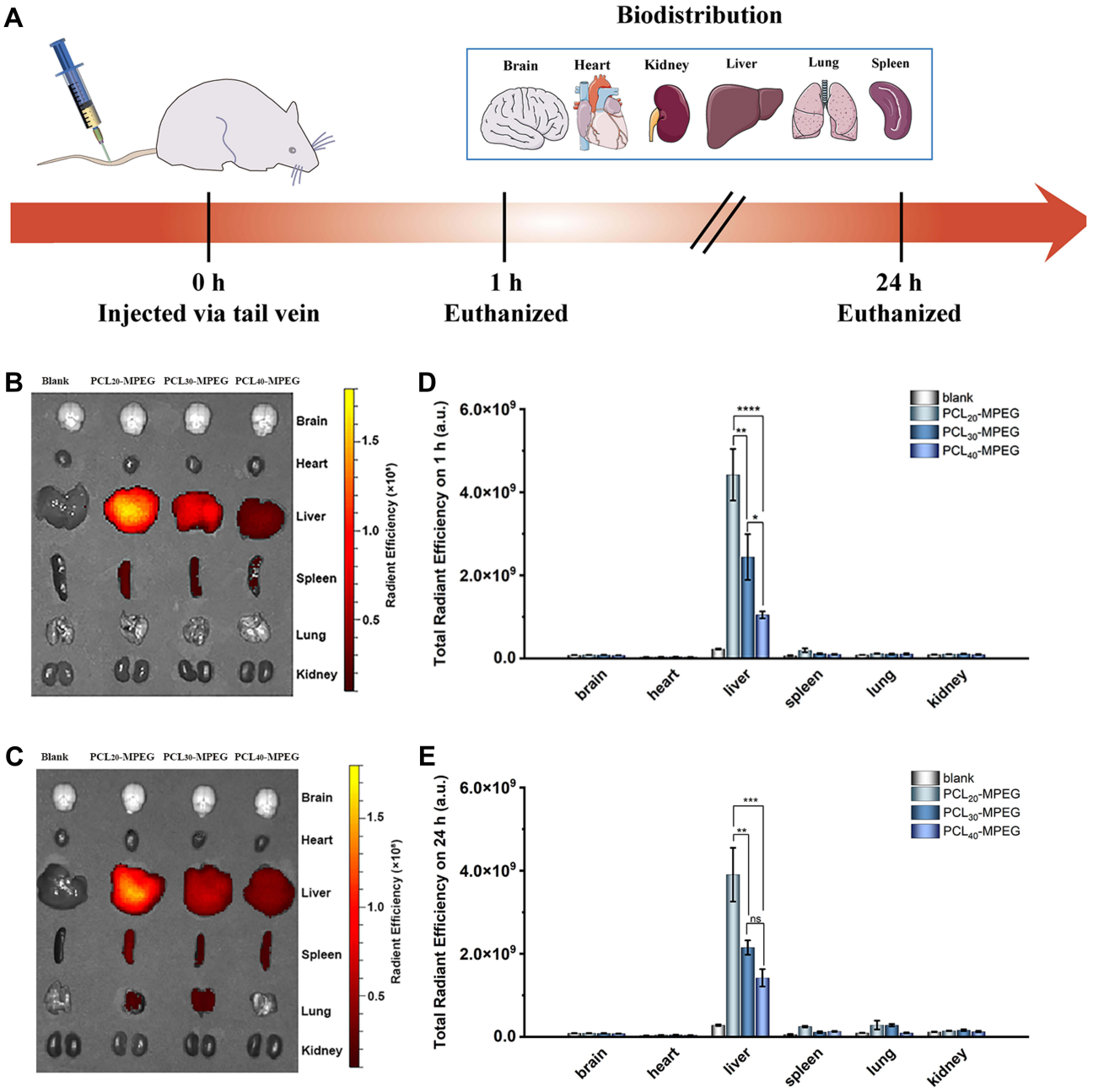

Figure 11 (**A**) The schematic illustration of the experimental schedule. The images of the PCL_n-MPEG micelles biodistribution after injected into blood 1h (**B**) and 24h (**C**). The fluorescence intensities of the micelles biodistribution 1h (**D**) and 24h (**E**). (n=3, *p <0.05, **p <0.01, ***p <0.005, ****p <0.0001).
Abbreviation: ns, no significant difference.

in heart and kidney tissues.[48] In contrast, as three major organs of RES or MPS, liver, spleen, and lungs had significantly higher uptake than other organs, where liver had the highest accumulation compared with that in spleen and lungs, which probably due to that liver is a huge MPS organ containing considerable number of unique macrophages, Kupffer cells.[49] For the three micelles, the accumulation levels in liver were also varied with different polymer constitutions, that was, PCL_{20}-MPEG had the highest radiant efficiency and highest uptake in liver at both two time points and followed by PCL_{30}-MPEG and PCL_{40}-MPEG. Differing to the results of phagocytosis in vitro, it was PCL_{40}-MPEG but not PCL_{30}-MPEG with the least phagocytosis had the lowest uptake by liver, suggested that in vivo circumstance provided more complex factors affected micellar biodistribution.

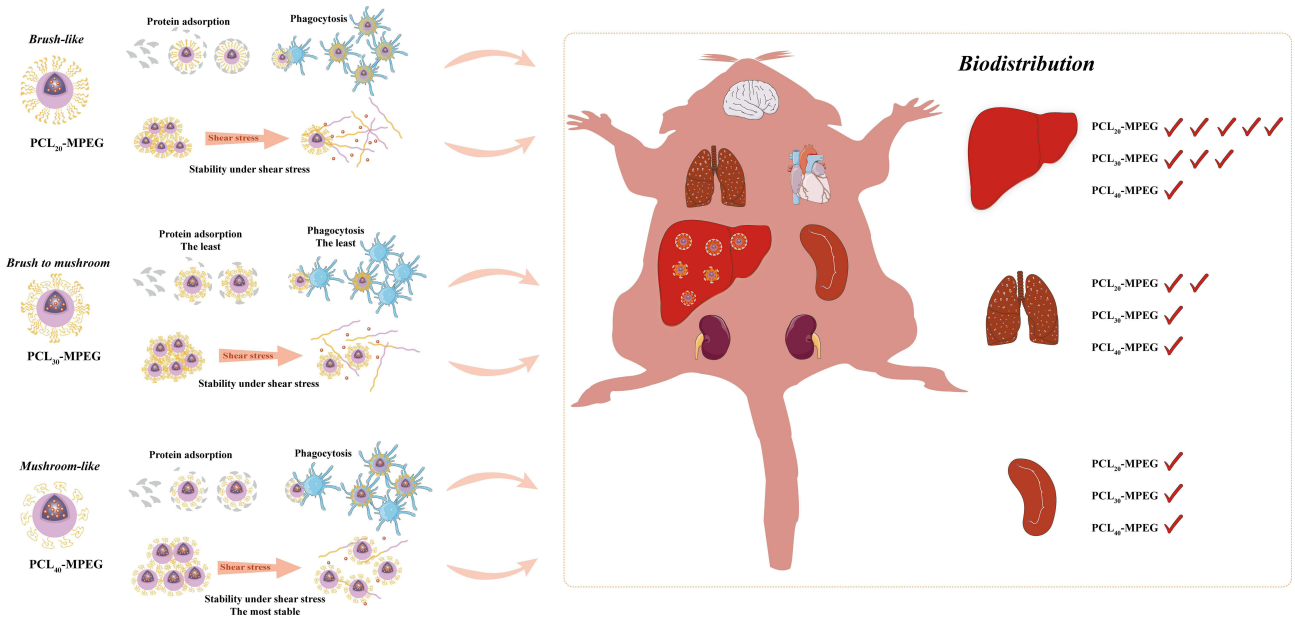

Figure 12 The schematic illustration of the proposed mechanism.

Mechanism Discussion

PEGylation has long been an effective strategy as an inert and antifouling shell for modulating the interactions between micelles and blood components, phagocytosis, and biodistribution. For example, several clinically relevant micelles such as PEG-PCL, PEG-PDLLA, and PEG-PLA are all PEGylated. The antifouling property of the PEG is derived from its hydrophilic molecular chains binding water to form a steric repulsion layer. Consistently, in our study, the three PCL-MPEG micelles showed no obviously effect on the red blood cells, platelet activation, and blood coagulation. However, the protein adsorption, phagocytosis, and biodistribution showed significant difference when PCL chain length was tuned. To explain these phenomena, mechanisms were proposed as follows (Figure 12) based on our results and literatures.

First, as our results and previous studies showed that the PEG density on micellar surface was decreased with the increasing of PCL chain length, which resulted in the forming "brush-like" conformation, decrease of the flexibility and steric repulsion, and increase of the protein adsorption for higher PEG coverage density, while lower surface PEG density increased the chain mobility formed "mushroom-like" conformation, led to incomplete coverage and uncovered spaces as "gaps" for protein adsorption. Therefore, there might be an optimal range of conformation between "brush-like" and "mushroom-like" where existed sufficient steric repulsion effect as well as appropriate coverage density which could effectively reduce proteins adsorption. In the present work, the PCL_{30}-MPEG micelles exhibited the lowest protein adsorption among three micelles, indicated that the conformation might in the optimal range as evidenced by DPD simulation.

The protein adsorption mediated the following specific recognition by MPS. The phagocytosis by macrophages in vitro showed that the PCL_{30}-MPEG micelles had the lowest phagocytosis, which was consistent with the result of protein adsorption. However, in vivo it was PCL_{40}-MPEG but not PCL_{30}-MPEG had the lowest uptake by liver. Besides phagocytosis, biodistribution of the micelles was also related with the stability of the micelles. Sun et al[25] found that proteins and shear stress together led to micellar dissociation and unimers were quickly sequestered by macrophages into liver. The micellar stability was expected to improve when high molecular weight PCL was used. The similar trend was investigated by Liu and co-workers[35] that longer PCL chains with higher crystallization and higher stability of micelles resulted micellar longer circulation. In deed, it had been observed in our study that with the increase of PCL chain length, the micellar stability gradually increased, implying that PCL_{40}-MPEG was more stable and this was well in line with the lowest sequestration level in liver. The distinct outcomes between in vitro and in vivo in this work indicated how the circumstances

in vivo was complex than in vitro, so that there were more factors would affect micellar blood circulation and biodistribution in actual application. Not only involve protein adsorption, phagocytosis, but also stability under shear stress.

Conclusion

In this work, a series of PCL-PEG copolymers with identical PEG and tunable PCL chain length were synthesized and self-assembled to micelles with different surface PEG coverage density and chain conformation from "mushroom-like" to "brush-like", in which doxorubicin was encapsulated as a model drug. The stability of the micelles was in the order of PCL_{40}- MPEG > PCL_{30}-MPEG > PCL_{20}-MPEG which was dependent on the PCL chain length. For blood components, the micelles have no significant effect on the red blood cells, blood coagulation, and platelet activation, while the protein adsorption and phagocytosis were affected differently, with both lowest adsorption and phagocytosis for PCL_{30}-MPEG with a conformation between "mushroom-like" and "brush-like". The in vivo biodistribution assay showed that the micelles mainly accumulated in liver, with the order consistent with their stability, indicating that, besides the phagocytosis, the stability of the micelle plays an important role in biodistribution as well. Based on above results, the mechanism was proposed and discussed.

Acknowledgments

This work was sponsored by the National Natural Science Foundation of China (No. 81401528 and 51873122), Sichuan Province Science and Technology Project (No. 2020YFH0096), the funding of Chengdu Science and Technology Bureau (No. 2019-YF05-00511-SN), and the funding of West China Hospital, Sichuan University (HX2019nCoV041).

Disclosure

The authors report no conflicts of interest for this work.

References

1. Huang L, Huang J, Huang J, et al. Nanomedicine - a promising therapy for hematological malignancies. *Biomater Sci*. 2020;8(9):2376–2393. doi:10.1039/D0BM00129E
2. Zhang H, Dong S, Li Z, et al. Biointerface engineering nanoplatforms for cancer-targeted drug delivery. *Asian J Pharm Sci*. 2020;15(4):397–415. doi:10.1016/j.ajps.2019.11.004
3. Tang L, Mei Y, Shen Y, et al. Nanoparticle-Mediated Targeted Drug Delivery to Remodel Tumor Microenvironment for Cancer Therapy. *Int J Nanomedicine*. 2021;16:5811–5829. doi:10.2147/IJN.S321416
4. Xu M, Yao C, Zhang W, Gao S, Zou H, Gao J. Anti-Cancer Activity Based on the High Docetaxel Loaded Poly(2-Oxazoline)s Micelles. *Int J Nanomedicine*. 2021;16:2735–2749. doi:10.2147/IJN.S298093
5. You X, Wang L, Wang L, Wu J. Rebirth of Aspirin Synthesis By-Product: prickly Poly(salicylic acid) Nanoparticles as Self-Anticancer Drug Carrier. *Adv Funct Mater*. 2021;31(33):2100805. doi:10.1002/adfm.202100805
6. Park IH, Sohn JH, Kim SB, et al. An Open-Label, Randomized, Parallel, Phase III Trial Evaluating the Efficacy and Safety of Polymeric Micelle-Formulated Paclitaxel Compared to Conventional Cremophor EL-Based Paclitaxel for Recurrent or Metastatic HER2-Negative Breast Cancer. *Cancer Res Treat*. 2017;49(3):569–577. doi:10.4143/crt.2016.289
7. Majumder N, G Das N, Das SK. Polymeric micelles for anticancer drug delivery. *Ther Deliv*. 2020;10:613–635. doi:10.4155/tde-2020-0008
8. Ding J, Chen J, Gao L, et al. Engineered nanomedicines with enhanced tumor penetration. *Nano Today*. 2019;29:100800. doi:10.1016/j.nantod.2019.100800
9. Blanco E, Shen H, Ferrari M. Principles of nanoparticle design for overcoming biological barriers to drug delivery. *Nat Biotechnol*. 2015;33(9):941–951. doi:10.1038/nbt.3330
10. Lima T, Bernfur K, Vilanova M, Cedervall T. Understanding the Lipid and Protein Corona Formation on Different Sized Polymeric Nanoparticles. *Sci Rep*. 2020;10(1):1129. doi:10.1038/s41598-020-57943-6
11. Allouni ZE, Gjerdet NR, Cimpan MR, Hol PJ. The effect of blood protein adsorption on cellular uptake of anatase TiO2 nanoparticles. *Int J Nanomedicine*. 2015;10:687–695. doi:10.2147/IJN.S72726
12. Lu Y, Zhang E, Yang J, Cao Z. Strategies to improve micelle stability for drug delivery. *Nano Res*. 2018;11(10):4985–4998. doi:10.1007/s12274-018-2152-3
13. Aggarwal P, Hall JB, McLeland CB, Dobrovolskaia MA, McNeil SE. Nanoparticle interaction with plasma proteins as it relates to particle biodistribution, biocompatibility and therapeutic efficacy. *Adv Drug Deliv Rev*. 2009;61(6):428–437. doi:10.1016/j.addr.2009.03.009
14. Cedervall T, Lynch I, Lindman S, Berggard T, Thulin E. Understanding the nanoparticle-protein Corona using methods to quantify exchange rates and affinities of proteins for nanoparticles. *Proc Natl Acad Sci*. 2007;7:2050–2055. doi:10.1073/pnas.0608582104
15. Forest V, Pourchez J. Preferential binding of positive nanoparticles on cell membranes is due to electrostatic interactions: a too simplistic explanation that does not take into account the nanoparticle protein Corona. *Mater Sci Eng C Mater Biol Appl*. 2017;70(Pt 1):889–896. doi:10.1016/j.msec.2016.09.016
16. Dos Santos SN, Rezen de Dos Reis SR, Pires LP, et al. Avoiding the mononuclear phagocyte system using human albumin for mesoporous silica nanoparticle system. *Microporous Mesoporous Mater*. 2017;251:181–189. doi:10.1016/j.micromeso.2017.06.005

17. Wang JL, Du XJ, Yang JX, et al. The effect of surface poly(ethylene glycol) length on in vivo drug delivery behaviors of polymeric nanoparticles. *Biomaterials*. 2018;182:104–113. doi:10.1016/j.biomaterials.2018.08.022
18. Fan Z, Zhu P, Zhu Y, Wu K, Li CY, Cheng H. Engineering long-circulating nanomaterial delivery systems. *Curr Opin Biotechnol*. 2020;66:131–139. doi:10.1016/j.copbio.2020.07.006
19. Baboci L, Capolla S, Di Cintio F, et al. The Dual Role of the Liver in Nanomedicine as an Actor in the Elimination of Nanostructures or a Therapeutic Target. *J Oncol*. 2020;2020:4638192. doi:10.1155/2020/4638192
20. Hwang D, Ramsey JD, Kabanov AV. Polymeric micelles for the delivery of poorly soluble drugs: from nanoformulation to clinical approval. *Adv Drug Deliv Rev*. 2020;156:80–118. doi:10.1016/j.addr.2020.09.009
21. Wang X, Yang C, Wang C, et al. Polymeric micelles with alpha-glutamyl-terminated PEG shells show low non-specific protein adsorption and a prolonged in vivo circulation time. *Mater Sci Eng C Mater Biol Appl*. 2016;59:766–772. doi:10.1016/j.msec.2015.10.084
22. Zhou H, Fan Z, Li PY, et al. Dense and Dynamic Polyethylene Glycol Shells Cloak Nanoparticles from Uptake by Liver Endothelial Cells for Long Blood Circulation. *ACS Nano*. 2018;12(10):10130–10141. doi:10.1021/acsnano.8b04947
23. Zahr AS, Davis CA, Pishko MV. Macrophage Uptake of Core-Shell Nanoparticles Surface Modified with Poly(ethylene glycol). *Langmuir*. 2006;19:8178–8185. doi:10.1021/la060951b
24. Owens DE 3rd, Peppas NA. Opsonization, biodistribution, and pharmacokinetics of polymeric nanoparticles. *Int J Pharm*. 2006;307(1):93–102. doi:10.1016/j.ijpharm.2005.10.010
25. Sun X, Wang G, Zhang H, et al. The Blood Clearance Kinetics and Pathway of Polymeric Micelles in Cancer Drug Delivery. *ACS Nano*. 2018;12(6):6179–6192. doi:10.1021/acsnano.8b02830
26. Chu C, Xiang Z, Wang J, Xie H, Xiang T, Zhou S. A near-infrared light-triggered shape-memory polymer for long-time fluorescence imaging in deep tissues. *J Mater Chem B*. 2020;8(35):8061–8070. doi:10.1039/D0TB01237H
27. Yang C, Yuan C, Liu W, et al. DPD studies on mixed micelles self-assembled from MPEG-PDEAEMA and MPEG-PCL for controlled doxorubicin release. *Colloids Surf B Biointerfaces*. 2019;178:56–65. doi:10.1016/j.colsurfb.2019.02.043
28. Guo X, Sun T, Zhong R, et al. Effects of Chitosan Oligosaccharides on Human Blood Components. *Front Pharmacol*. 2018;9:1412. doi:10.3389/fphar.2018.01412
29. Shuai XT, Merdan T, Schaper AK, Xi F, Kissel T. Core-Cross-Linked Polymeric Micelles as Paclitaxel.pdf. *Bioconjug Chem*. 2004;3:441–448. doi:10.1021/bc034113u
30. Lin WJ, Nie SY, Chen Q, Qian Y, Wen XF, Zhang LJ. Structure-property relationship of pH-sensitive (PCL)2(PDEA-b-PPEGMA)2micelles: experiment and DPD simulation. *AiChE J*. 2014;60(10):3634–3646. doi:10.1002/aic.14562
31. Sliozberg YR, Gair JL, Hsieh AJ. Dissipative particle dynamics simulation of microphase separation in polyurethane urea nanocomposites. *Polymer*. 2020;193:122339. doi:10.1016/j.polymer.2020.122339
32. Du XJ, Wang JL, Liu WW, et al. Regulating the surface poly(ethylene glycol) density of polymeric nanoparticles and evaluating its role in drug delivery in vivo. *Biomaterials*. 2015;69:1–11. doi:10.1016/j.biomaterials.2015.07.048
33. Shiraishi K, Sanada Y, Mochizuki S, et al. Determination of polymeric micelles' structural characteristics, and effect of the characteristics on pharmacokinetic behaviors. *J Control Release*. 2015;203:77–84. doi:10.1016/j.jconrel.2015.02.017
34. Guo Z, Zhao K, Liu R, et al. pH-sensitive polymeric micelles assembled by stereocomplexation between PLLA-b-PLys and PDLA-b-mPEG for drug delivery. *J Mater Chem B*. 2019;7:334–345. doi:10.1039/C8TB02313A
35. Liu Y, Fens M, Capomaccio RB, et al. Correlation between in vitro stability and pharmacokinetics of poly(epsilon-caprolactone)-based micelles loaded with a photosensitizer. *J Control Release*. 2020;328:942–951. doi:10.1016/j.jconrel.2020.10.040
36. Zhen Z, Liu X, Huang T, Xi T, Zheng Y. Hemolysis and cytotoxicity mechanisms of biodegradable magnesium and its alloys. *Mater Sci Eng C Mater Biol Appl*. 2015;46:202–206. doi:10.1016/j.msec.2014.08.038
37. Muravyov A, Tikhomirova I. Signaling pathways regulating red blood cell aggregation. *Biorheology*. 2014;51:135–145. doi:10.3233/BIR-140664
38. Yang Y, Li X, Qiu H, et al. Polydopamine Modified TiO2 Nanotube Arrays for Long-Term Controlled Elution of Bivalirudin and Improved Hemocompatibility. *ACS Appl Mater Interfaces*. 2018;10(9):7649–7660. doi:10.1021/acsami.7b06108
39. Tu Q, Shen X, Liu Y, et al. A facile metal–phenolic–amine strategy for dual-functionalization of blood-contacting devices with antibacterial and anticoagulant properties. *Mater Chem Front*. 2019;3(2):265–275. doi:10.1039/C8QM00458G
40. Singh N, Marets C, Boudon J, Millot N, Saviot L, Maurizi L. In vivo protein Corona on nanoparticles: does the control of all material parameters orient the biological behavior? *Nanoscale Adv*. 2021;3(5):1209–1229. doi:10.1039/D0NA00863J
41. Chen D, Ganesh S, Wang W, Amiji M. Plasma protein adsorption and biological identity of systemically administered nanoparticles. *Nanomedicine*. 2017;17:2113–2135. doi:10.2217/nnm-2017-0178
42. Qie Y, Yuan H, von Roemeling CA, et al. Surface modification of nanoparticles enables selective evasion of phagocytic clearance by distinct macrophage phenotypes. *Sci Rep*. 2016;6:26269. doi:10.1038/srep26269
43. Binnemars-Postma KA, ten Hoopen HW, Storm G, Prakash J. Differential uptake of nanoparticles by human M1 and M2 polarized macrophages: protein Corona as a critical determinant. *Nanomedicine*. 2016;22:2889–2902. doi:10.2217/nnm-2016-0233
44. Zheng P, Liu Y, Chen J, Xu W, Li G, Ding J. Targeted pH-responsive polyion complex micelle for controlled intracellular drug delivery. *Chin Chem Lett*. 2020;31(5):1178–1182. doi:10.1016/j.cclet.2019.12.001
45. Cheng WJ, Lin SY, Chen M, et al. Active Tumoral/Tumor Environmental Dual-Targeting by Non-Covalently Arming with Trispecific Antibodies or Dual-Bispecific Antibodies on Docetaxel-Loaded mPEGylated Nanocarriers to Enhance Chemotherapeutic Efficacy and Minimize Systemic Toxicity. *Int J Nanomedicine*. 2021;16:4017–4030. doi:10.2147/IJN.S301237
46. Maeda H. Toward a full understanding of the EPR effect in primary and metastatic tumors as well as issues related to its heterogeneity. *Adv Drug Deliv Rev*. 2015;91:3–6. doi:10.1016/j.addr.2015.01.002
47. Bae YH, Park K. Targeted drug delivery to tumors: myths, reality and possibility. *J Control Release*. 2011;153:198–205. doi:10.1016/j.jconrel.2011.06.001
48. Chung EJ, Mlinar LB, Sugimoto MJ, Nord K, Roman BB, Tirrell M. In vivo biodistribution and clearance of peptide amphiphile micelles. *Nanomedicine*. 2015;11(2):479–487. doi:10.1016/j.nano.2014.08.006
49. Nie S. Understanding and overcoming major barriers in cancer nanomedicine. *Nanomedicine*. 2010;5(4):523–528. doi:10.2217/nnm.10.23